Available online at website: https://journal.bcrec.id/index.php/bcrec

Bulletin of Chemical Reaction Engineering & Catalysis, 19 (3) 2024, 442-454

Research Article

Modulation of the Microstructure and Enhancement of the Photocatalytic Performance of g-C_3N_4 by Thermal Exfoliation

Xinshan Zhao[1], Junwei Yu[2], Tingyu Meng[2], Yuanyuan Luo[1], Yanzhen Fu[2], Zhao Li[2], Lin Tian[2], Limei Sun[2], Jing Li[2,*]

[1]School of Chemistry and Chemical Engineering, Yili Normal University, 835000, Yining, China.
[2]School of Materials and Chemical Engineering, Xuzhou University of Technology, 221018, Xuzhou, China.

Received: 21st July 2024; Revised: 16th August 2024; Accepted: 16th August 2024
Available online: 8th September 2024; Published regularly: October 2024

Abstract

This work explores the impact of reaction temperature during thermal exfoliation treatment of bulk-g-C_3N_4 in the air atmosphere on the structure and performance of the resulting CN photocatalyst. The analysis conducted using XRD, FT-IR, XPS, SEM, and elements mapping tests, illustrated an increase in nitrogen-vacancy and oxygen content on the surface of the CN photocatalyst, resulting in a porous and sparse structure, changes in crystal size, and improved visible light absorption performance. The photocatalytic reduction experiments of hexavalent chromium (Cr(VI)) showed that the CN-540 showed the highest reduction rate of 96.9%, with a reaction rate constant 6.21 times that of bulk-g-C_3N_4. After 100 min of illumination, the photocatalytic degradation rates of CN-540 for TC-HCl and RhB were 66.7% and 60.6%, respectively. The TOC test results indicated mineralization rates of 51.5% for TC-HCl and 46.6% for RhB. Room temperature fluorescence spectroscopy (PL), transient photocurrent response (TPC), and electrochemical impedance spectroscopy (EIS) measurements confirmed the excellent photogenerated charge carrier separation and transport efficiency of CN-540. The photocatalytic mechanism for reducing Cr(VI) by CN-540 was elucidated based on the active species ·OH and $\cdot O_2^-$ and Mott-Schottky (M-S) tests. This study provides experimental data for optimizing the photocatalytic performance of g-C_3N_4 and paves a new way for developing efficient photocatalysts.

Keywords: Graphitic Carbon Nitride; Thermal Exfoliation; Photocatalytic Reduction; Cr(VI); Photo-induced Charge Carriers

How to Cite: X. Zhao, J. Yu, T. Meng, Y. Luo, Y. Fu, Z. Li, L. Tian, L. Sun, J. Li (2024). Modulation of the Microstructure and Enhancement of the Photocatalytic Performance of g-C_3N_4 by Thermal Exfoliation. *Bulletin of Chemical Reaction Engineering & Catalysis*, 19 (3), 442-454 (doi: 10.9767/bcrec.20189)

Permalink/DOI: https://doi.org/10.9767/bcrec.20189
Supporting Information: https://journal.bcrec.id/index.php/bcrec/article/downloadSuppFile/20189/5264

1. Introduction

As industrialization progresses, environmental pollution issues, particularly those involving heavy metal ion contamination, have become an increasingly severe global challenge. Hexavalent chromium (Cr(VI)) is a typical heavy metal pollutant that mainly originates from the wastewater discharge of industries such as leather processing, electroplating, printing, and pigments [1–2]. Due to its high toxicity, high water solubility, and resistance to degradation, Cr(VI) not only extensively exists in the environment but also forms free radicals, posing a significant threat to ecology and human health [1–2]. In aquatic environments, chromium mainly exists in the less toxic trivalent form Cr(III) and the highly toxic hexavalent form Cr(VI), with the toxicity of Cr(VI) being approximately 1000 times that of Cr(III) [3].

Current Cr(VI) treatment technologies include adsorption, membrane filtration, ion exchange, biotechnology, chemical reduction, and electrochemical treatment [1–6]. Although these technologies effectively remove Cr(VI) to a certain

* Corresponding Author.
Email: lijingxz111@163.com (J. Li)

extent, they are often accompanied by high costs, high energy consumption, and the potential for secondary pollution. Therefore, it is particularly important to develop a treatment technology that is both economical and environmentally friendly. Photocatalytic technology, which can utilize the energy of natural sunlight to drive the reaction of Cr(VI), is characterized by low cost and environmental friendliness, showing its potential in treating Cr(VI) contamination. Therefore, through photocatalytic technology, Cr(VI) can be converted into less toxic Cr(III), making it an effective and environmentally friendly pollution control strategy [1–6].

However, photocatalytic technology still needs to improve in practical applications, mainly due to the need for high-performance, cost-effective, and environmentally friendly photocatalysts. Therefore, the development of high-performance photocatalysts is an important research direction for the development of environmental science. Graphitic carbon nitride (g-C_3N_4) is a layered photocatalyst with remarkable photocatalytic potential, which possesses non-toxicity, good chemical stability, and a suitable band gap structure [7–12]. Nevertheless, due to disordered growth and interlayer intermolecular interactions, the conventional thermal polymerization method for preparing g-C_3N_4 makes the synthesized g-C_3N_4 usually present a bulk structure (bulk-g-C_3N_4). Its structural defects manifest in a small specific surface area, fewer surface active sites, and a high complexation rate of the photogenerated electron-hole pairs [7,8]. These factors limit its activity in visible light photocatalytic reactions [7–12]. Its structural defects manifest in a small specific surface area, fewer surface active sites, and a high complexation rate of the photogenerated electron-hole pairs [7,8]. These factors limit its activity in visible light photocatalytic reactions [7–12].

Recent investigations have employed various strategies to enhance the performance of g-C_3N_4 to address these limitations, including morphological control [9], doping modification [8, 10], heterojunction construction [11–14], chemical and thermal exfoliation [15-17], and dye sensitization [18]. For instance, Yang *et al.* [8] successfully synthesized g-C_3N_4 nanosheets with excellent photocatalytic degradation performance for Rhodamine B through the synergistic effect of dual-element doping and secondary calcination. Nguyen *et al.* [11] prepared Ag/ZnO/g-C_3N_4 through a physical mixing calcination method, enhancing its visible light photocatalytic degradation activity for methylene blue (MB). Wang *et al.* [11] constructed a TiO_2@C/g-C_3N_4 heterojunction for efficient removal of NO. Zhang *et al.* [15] used an aqueous sodium hydroxide solution to treat g-C_3N_4 to improve its photocatalytic activity for reducing Cr(VI) under visible light. On the other hand, Medeiros *et al.* [16] examined the effects of chemical and thermal exfoliation on the physicochemical and optical properties of carbon nitride and the underlying reasons.

Based on the various modification methods for g-C_3N_4, thermal exfoliation treatment has been widely studied for its simplicity, effectiveness, and minimal alteration of the material structure [8,17,19,20]. However, in the existing works, the heat treatment temperature is higher than 590 °C [19], and gas protection is required [20], increasing energy consumption and costs. Additionally, further research is necessary to apply photocatalytic reduction of heavy metals. In this work, we modulated the microstructure of g-C_3N_4 by low-temperature thermal exfoliation (500-540 °C) in air, obtaining the effects of thermal exfoliation temperature on grain size and bandgap structure. By comparing the visible-light photocatalytic reduction activity of bulk-g-C_3N_4 and CN for Cr(VI), combining electrochemical tests and band structure, we propose the mechanism of CN photocatalytic reduction of Cr(VI) and discuss the possible reasons for the enhanced photocatalytic activity.

2. Materials and Methods

2.1 Reagents

Dicyandiamide ($C_2H_4N_4$), diphenylcarbazide ($C_{13}H_{14}N_4O$), citric acid ($C_6H_8O_7$), potassium dichromate ($K_2Cr_2O_7$), acetone (C_3H_6O), sulfuric acid (H_2SO_4), and anhydrous ethanol (C_2H_6O). All chemical reagents are of analytical grade and were purchased from Sinopharm Chemical Reagent Co. and were used without further purification.

2.2 Synthesis

Weigh 3 g of dicyandiamide, place it into a capped crucible, and then put it into a muffle furnace. Heat it at a rate of 10 °C/min to a reaction temperature of 540 °C for 2 h. The resulting product is denoted as bulk-g-C_3N_4. The homemade bulk-g-C_3N_4 was put into a muffle furnace again and heated at 500 °C, 520 °C, and 540 °C with the same heating rate for 2 h. The products were labeled as CN-500, CN-520, and CN-540. It should be noted that as the temperature increases, the yield of CN obtained by thermal oxidation decreases. Considering the yield factor, select a temperature of up to 540 °C.

2.3 Characterizations

The composition of the synthesized materials was analyzed using an X-ray powder diffractometer (XRD, Ultima IV X, Rigaku

Corporation, Japan), a Fourier-transform infrared spectrometer (FT-IR, ALPHA, Bruker, Germany), and an X-ray photoelectron spectrometer (XPS, Thermo escalab 250 XI, Thermo Fisher Scientific, USA). The morphological characteristics of the materials were obtained using a scanning electron microscope (SEM, SU8600, Hitachi, Japan). The ultraviolet-visible-near-infrared diffuse reflectance spectrum of the synthesized photocatalyst was obtained using a UV-Vis DRS spectrometer (Lambda750, PerkinElmer, USA). The optical properties of the samples were measured using a photoluminescence spectrometer (PL, F-2700, Hitachi, Japan). Transient photocurrent response curves (*i-t*), electrochemical impedance spectroscopy (EIS), and Mott-Schottky (M-S) curves were obtained using an electrochemical workstation (CHI 660E, Chenhua Instruments Co., Ltd., Shanghai, China, using a three-electrode system with Ag/AgCl as the reference electrode). The mineralization rate of organic pollutants was measured by total organic carbon/total nitrogen tester (TOC, Model TNM-L, Shimadzu, Japan).

2.4 Cr(VI) Reduction Experiments

The experiments for the visible-light photocatalytic reduction of aqueous Cr(VI) by g-C_3N_4 were conducted using a GHX-Z photochemical reaction apparatus. The experimental conditions were as follows: a 250 W Xe lamp (filtered to remove UV light with wavelengths less than 420 nm), a reaction temperature of 25 °C, with 1 mL of 0.5 mol/L citric acid as the hole scavenger, and 300 mg of photocatalyst added to 300 mL of 10 mg/L $K_2Cr_2O_7$ solution. First, an adsorption-desorption experiment was carried out for 40 min in the dark. During the photocatalytic reaction after turning on the light source, the reaction solution was pipetted at fixed intervals, and the post-reaction clarified Cr(VI) solution was obtained by filtering through a fiber filter membrane with a pore size of 0.22 μm. The concentration of the aqueous Cr(VI) was determined using a spectrophotometer. The removal rate of Cr(VI) was obtained using Equation (1). In the equation, c_0 and c_t represent the concentration of aqueous Cr(VI) at 0 and t min, respectively.

$$R\ (\%) = \frac{c_0 - c_t}{c_0} \times 100\% \quad (1)$$

2.5 TC-HCl and RhB Degradation Experiments

The selective experiments of CN-540 were conducted through adsorption and photocatalytic experiments of 10 mg/L TC-HCl and RhB, with experimental parameters consistent with those of Cr(VI) reduction experiments. Rhodamine B (RhB) is an artificially synthesized rose-red, cationic dye commonly found in industrial wastewater from printing, textile, and food industries and is a common pollutant in such wastewater [21,22]. Tetracycline hydrochloride is a water-soluble polar compound and a widely used antimicrobial drug in clinical settings. Due to the low effective utilization rate of tetracycline hydrochloride (TC-HCl), 75% of it is excreted as metabolites [23], posing a threat to human health and the ecological environment. Given the high chemical stability of TC-HCl and RhB [21], these organic pollutants are typically not directly oxidized by O_2 in the air. Utilizing photocatalytic technology to purify organic wastewater is a potentially feasible strategy [21,24].

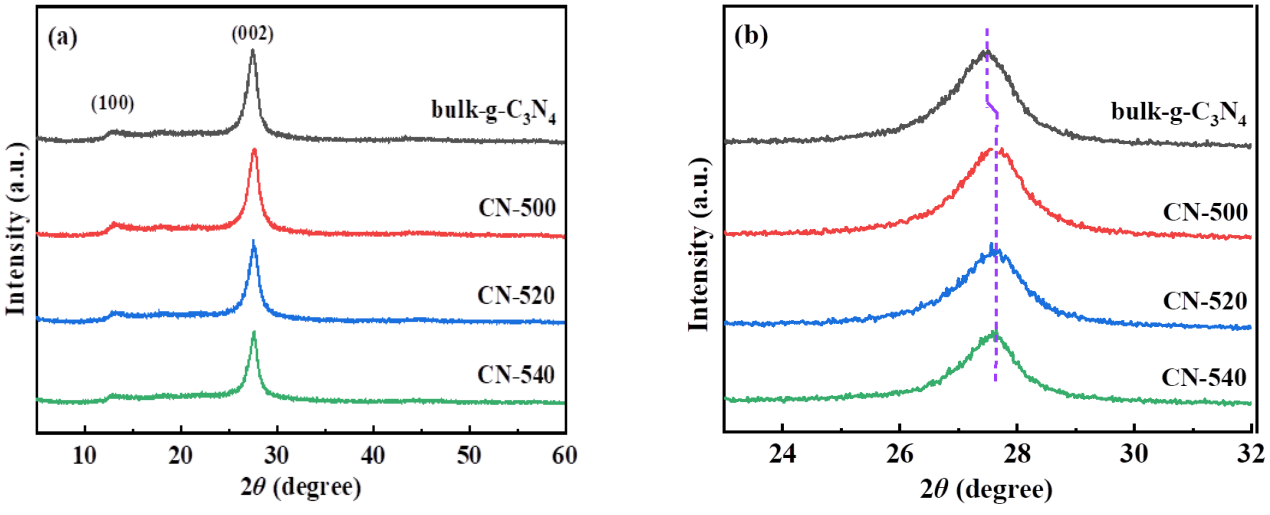

Figure 1. (a) XRD patterns of bulk-g-C_3N_4, CN-500, CN-520, and CN-540, (b) Enlarged view of the diffraction angles corresponding to the (002) plane.

3. Results and Discussion

3.1 Structural and Compositional Characterization

Figure 1 shows the XRD patterns of bulk-g-C_3N_4, and CN obtained through thermal exfoliation. Compared with the standard card (JCPDS 87-1526) [8], all samples exhibit the two characteristic peaks of graphitic carbon nitride. The strong peak at 27.4° is attributed to the (002) plane of graphitic carbon nitride, formed by stacking aromatic rings [17,25]. The weaker peak at 13.1° belongs to the 3-s-triazine units within the planar structure, corresponding to the (100) plane of g-C_3N_4 [17,25]. Notably, the diffraction angle of bulk-g-C_3N_4 on the (002) plane is 27.47°, while the diffraction angle of the exfoliated CN photocatalyst on the same plane is 27.64°. According to the change of diffraction angle and Equation (2) [26], it can be inferred that the interlayer spacing decreases.

$$2d = \frac{n \times \lambda}{\sin\theta} \quad (2)$$

Figure 2(a) provides the FT-IR spectra of bulk-g-C_3N_4, CN-500, CN-520, and CN-540, which are similar to each other, indicating that the thermal exfoliation in the air atmosphere did not destroy the basic structure of g-C_3N_4. However, there are changes in the intensity of the characteristic peaks at the typical breathing vibration mode of the triazine ring at 810 cm^{-1}, as well as the vibrational modes of C–N hybridization within the range of 1200 cm^{-1} to 1400 cm^{-1} (Figure S1 Supporting Information). These variations are attributed to the adjustment of the interlayer spacing. The absorption peak observed at 810 cm^{-1} is characteristic of the bending vibration of the triazine ring [5,13,27]. The absorption bands in the range of 1200 cm^{-1} to 1600 cm^{-1} are typical of the stretching vibrations of the aromatic CN heterocycles, with absorption peaks at 1230 cm^{-1}, 1315 cm^{-1}, and 1400 cm^{-1} attributed to the stretching vibrations of the aromatic C–N single bonds [5,13,27]. Additionally, the absorption peaks at 1560 cm^{-1} and 1629 cm^{-1} are attributed to the stretching

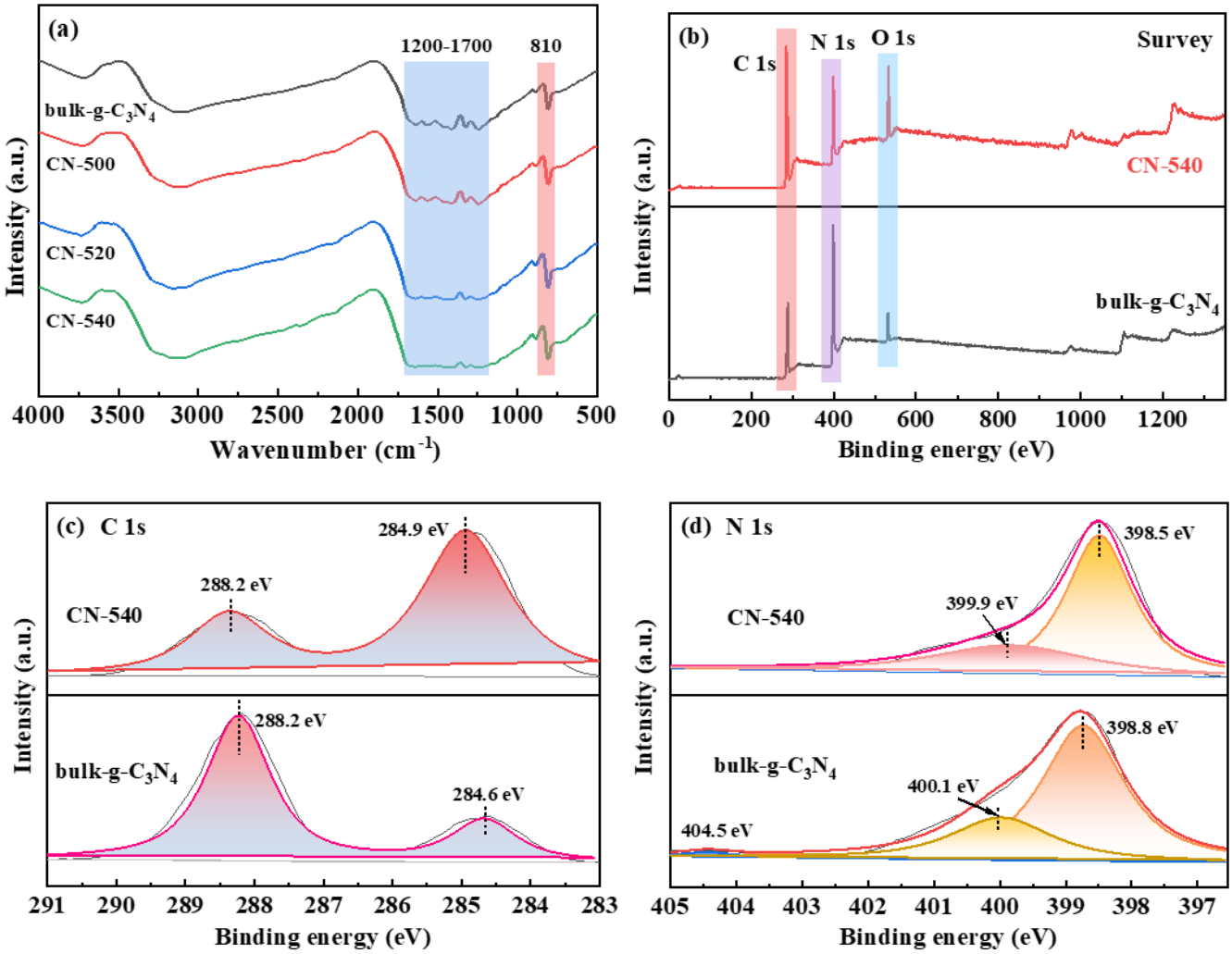

Figure 2. (a) FT-IR spectra of bulk-g-C_3N_4, CN-500, CN-520, and CN-540, (b) XPS survey, (c) C1s and (d) N1s of bulk-g-C_3N_4 and CN-540.

vibrations of −C=N and the stretching vibrations of C=O [5,13,27]. The broad absorption peak near 3200 cm^{-1} is attributed to the stretching vibrations of O−H or N−H bonds [17].

Using X-ray photoelectron spectroscopy (XPS) technology, we conducted a detailed analysis of the chemical states of elements on the surface of the photocatalyst. As shown in Figure 2(b), the survey spectrum indicates that both bulk-g-C_3N_4 and CN-540 consist of carbon (C), nitrogen (N), and oxygen (O) elements, with the presence of oxygen mainly due to the adsorption of CO_2 and H_2O on the surface of the photocatalyst. Further high-resolution XPS analysis shows that in Figure 2(c), the C1s peak is fitted to two peaks located at 288.2 eV and 284.9 eV, corresponding to the C−C bonds of adventitious carbon and the carbon atoms in the N=C−N_2 structure of the g-C_3N_4 molecular structure [10,13]. The N1s peak in Figure 2(d) is fitted to two peaks, with the binding energies at 398.5 eV and 399.9 eV for CN-540 corresponding to the nitrogen atoms in the sp^2 hybridized C=N−C bonds [20] and the nitrogen atoms in N−$(C)_3$, respectively. It is particularly noteworthy that compared to bulk-g-C_3N_4, the C1s binding energy of CN-540 is higher, while the N1s binding energy is lower. XPS peak separation software calculated the peak area of N1s spectra of bulk-g-C_3N_4 and CN-540. The N content of N−$(C)_3$ in CN-540 decreased from 29.4% to 24.3%. This experimental result suggests that during the thermal exfoliation process in the air atmosphere, CN-540 may have undergone the removal of nitrogen atoms, thereby introducing nitrogen

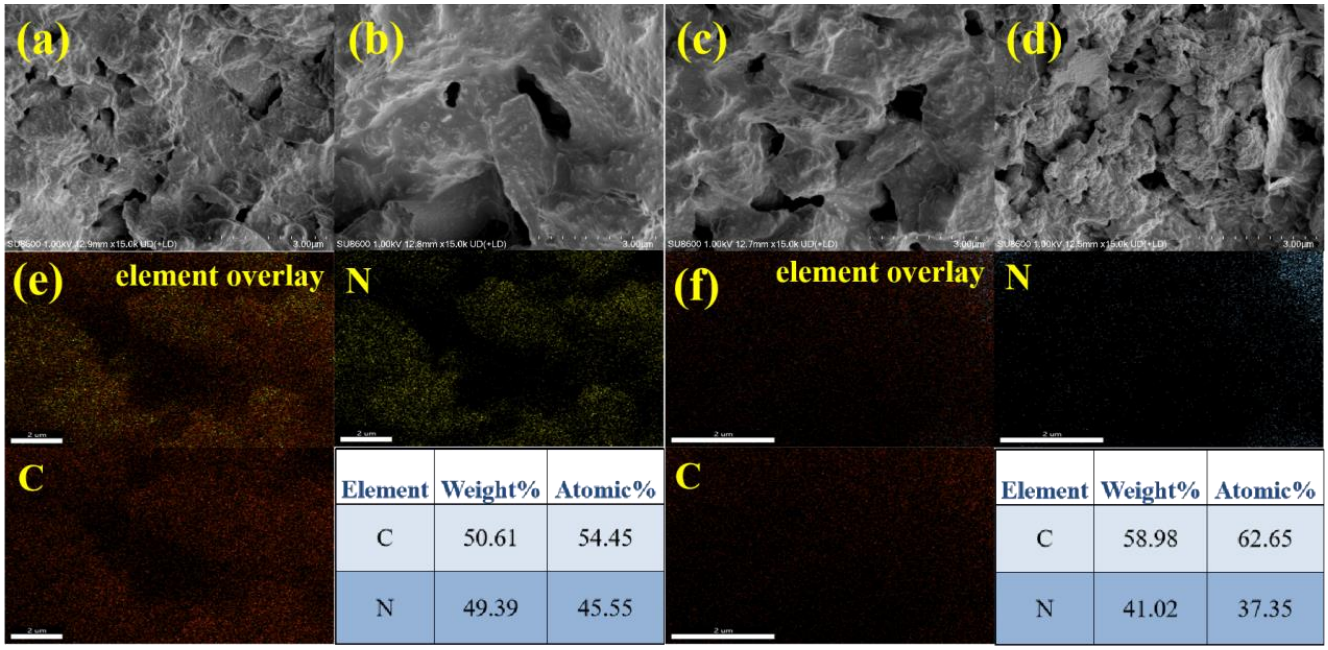

Element	Weight%	Atomic%
C	50.61	54.45
N	49.39	45.55

Element	Weight%	Atomic%
C	58.98	62.65
N	41.02	37.35

Figure 3. FESEM images of (a) bulk-g-C_3N_4, (b) CN-500, (c) CN-520, and (d) CN-540, EDX elemental mapping of (e) bulk-g-C_3N_4 and (f) CN-540.

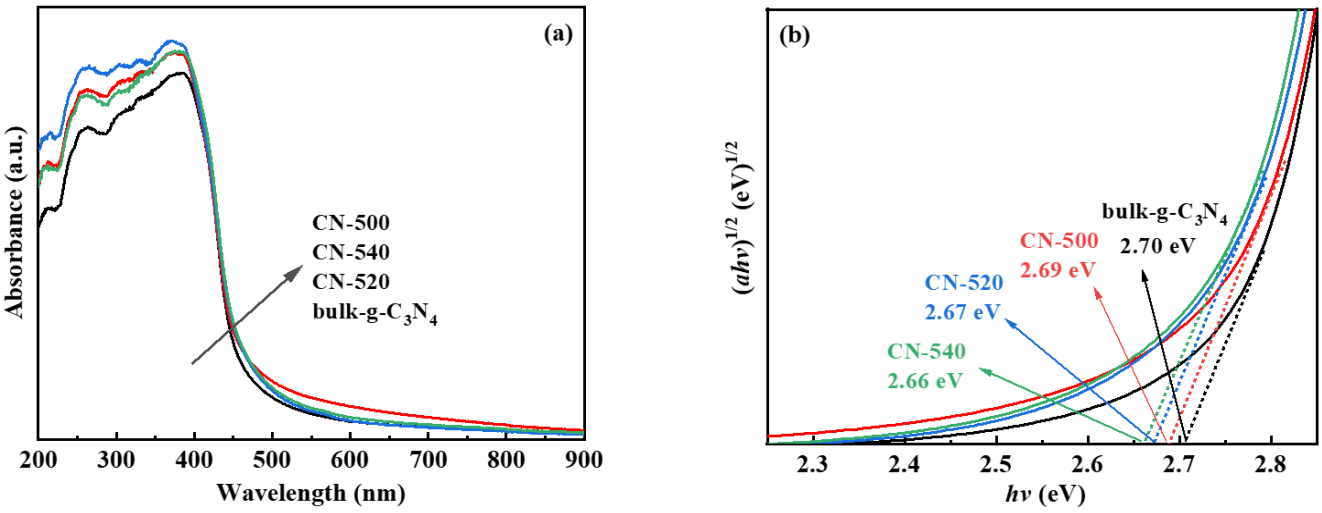

Figure 4. (a) UV-Vis spectra, (b) Band gap plots of bulk-g-C_3N_4, CN-500, CN-520, and CN-540.

vacancies [28,29], which could significantly affect the photocatalytic performance of the photocatalyst.

Figure 3 presents the SEM images of the prepared photocatalysts. Specifically, Figure 3(a) provides the morphology of bulk-g-C_3N_4, which exhibits a smooth bulk structure on its surface. Figures 3(b) to (d) display images of CN photocatalysts, indicating that as the temperature of thermal exfoliation treatment in the air

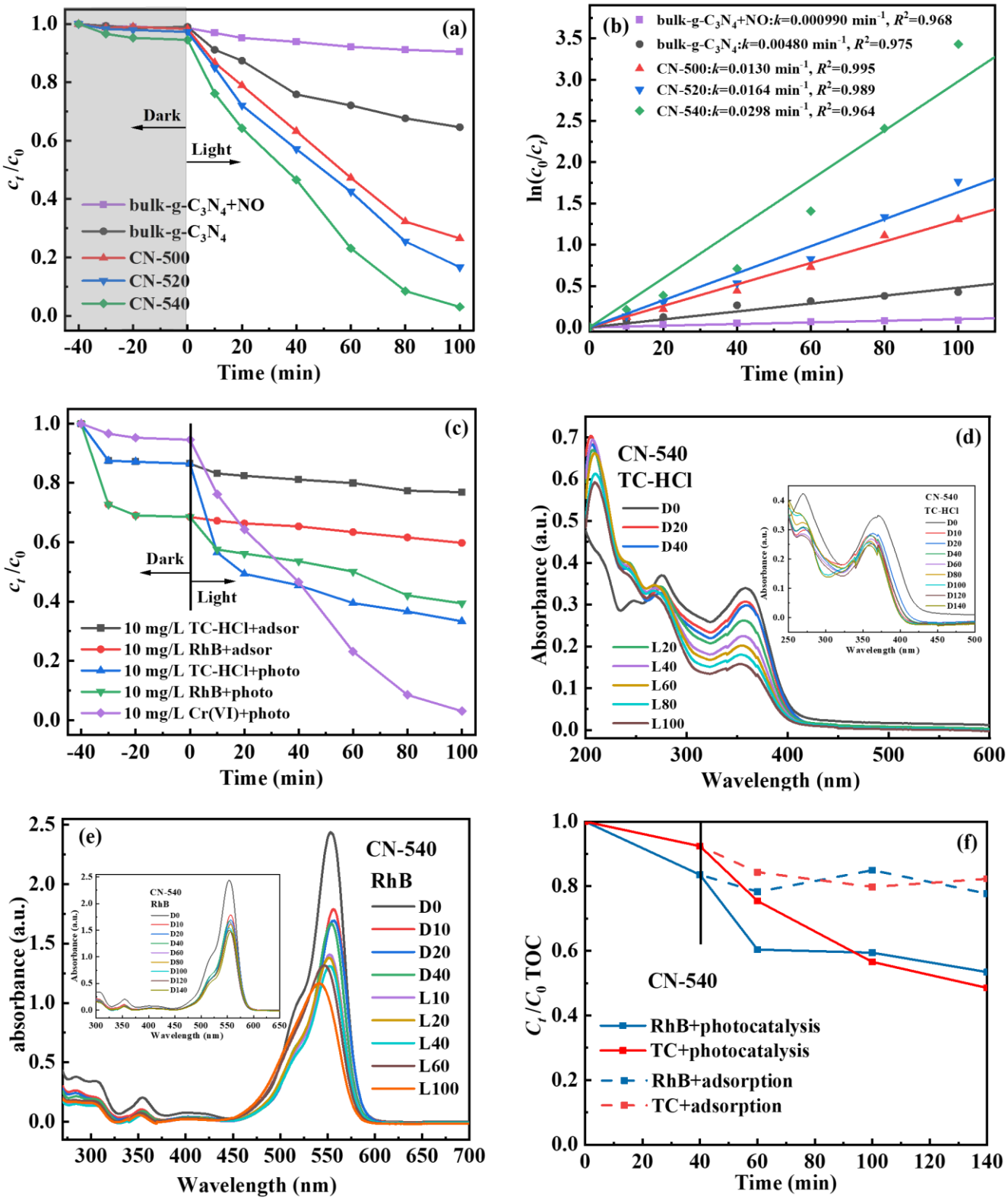

Figure 5. (a) Comparative activity chart of visible-light photocatalytic reduction of Cr(VI) by bulk-g-C_3N_4, CN-500, CN-520, and CN-540, (b) The pseudo-first-order reaction kinetics of samples, (c) Activity comparison of CN-540 for different pollutants, The UV-vise absorption spectra of CN-540 for the degradation and adsorption of organic pollutants (d) TC-HCl and (e) RhB, (f) The mineralization removal rate of TC-HCl and RhB by CN-540.

atmosphere increases, the degree of surface porosity and sponginess of CN increases. Figures 3(e) and 3(f) present the EDX elemental distribution maps for bulk-g-C_3N_4 and CN-540, respectively, showing the uniform distribution of C and N elements. The nitrogen content in CN-540 has decreased from 45.55% to 37.35%, indicating the removal of nitrogen atoms from the structure of these materials.

Ultraviolet-visible diffuse reflectance absorption spectroscopy is an excellent means of evaluating the light-harvesting ability of photocatalysts. Figure 4(a) shows the UV-Vis spectra of bulk-g-C_3N_4, CN-500, CN-520, and CN-540, where CN-500, CN-520, and CN-540 all exhibit enhanced visible light absorption compared to the bulk-g-C_3N_4. g-C_3N_4 is an indirect band gap semiconductor [13], by plotting $(ahv)^{1/2}$ versus (hv) [13], Figure 4(b) can be obtained. Extrapolating the linear part of the figure to $y = 0$ obtains the band gap energies for bulk-g-C_3N_4, CN-500, CN-520, and CN-540, which are 2.70 eV, 2.69 eV, 2.67 eV, and 2.66 eV, respectively. It can be seen that the bandgap energies of CN-500, CN-520, and CN-540 are all smaller than that of bulk-g-C_3N_4, and the bandgap energy decreases with the increase in thermal exfoliation temperature.

3.2 Photocatalytic Performance

Figure 5(a) compares the activity of the prepared photocatalysts in the visible-light photocatalytic reduction of the Cr(VI) process with citric acid added as a hole scavenger. The experimental results showed that increased irradiation time decreased the Cr(VI) concentration (Figure S2 Supporting Information). The photocatalytic reduction rates of Cr(VI) by bulk-g-C_3N_4, CN-500, CN-520, and CN-540 were 35.4%, 73.5%, 83.3%, and 96.9%, respectively, at 100 min. In contrast, the Cr(VI) reduction rate by bulk-g-C_3N_4 without citric acid was only 9.5% under the same conditions. This indicates that the photocatalytic performance of g-C_3N_4 can be improved by thermal exfoliation in the air atmosphere.

A pseudo-first-order kinetic equation (Eq. 3) was employed to further analyze the photocatalytic reduction process. Based on the relationship between $\ln(c_{i0}/c_{it})$ and t shown in Figure 5(b), the reaction rate constants for the photocatalytic reduction of Cr(VI) by different catalysts were determined. The results show that the photocatalytic reaction rate constant for CN-540 on Cr(VI) is about 0.0298 min^{-1}, 6.21 times that of bulk-g-C_3N_4, indicating a faster reaction rate.

$$\ln\left(\frac{c_{i0}}{c_{it}}\right) = kt \tag{3}$$

where, c_{it} and c_{i0} denote the concentration of Cr(VI) solution when the light irradiation time is t and 0 min, respectively.

Figures 5(c-e) show the comparative activity of CN-540 in treating different pollutants. The photocatalytic degradation rates of CN-540 for tetracycline hydrochloride (TC-HCl) and rhodamine B (RhB) are 66.7% and 60.6%, respectively. According to the experimental results shown in Figure 5(d), we observed that during the photocatalytic degradation of TC-HCl by CN-540, the concentration of the remaining TC-HCl in the solution gradually decreased with the increase of illumination time, and a slight shift of the absorption peak towards a smaller wavelength occurred near 360 nm. The inset of Figure 5(d) demonstrates the adsorption and removal of TC-HCl (23.1%) by CN-540 under dark conditions within 140 min. During this period, the change in absorbance of TC-HCl was prolonged, and the position of the absorption peak near 360

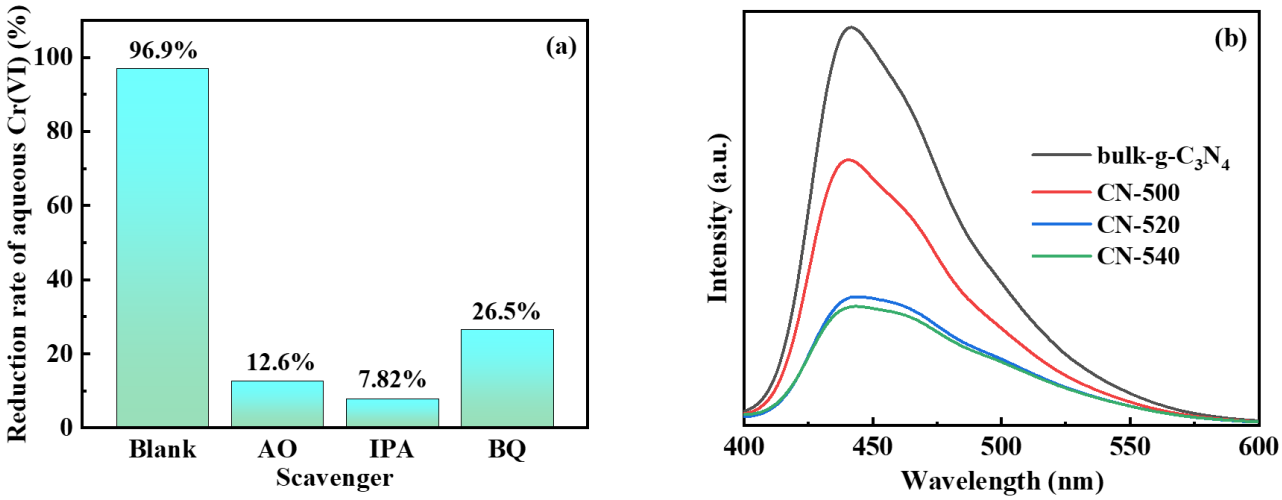

Figure 6. (a) Radical trapping experiment, and (b) PL spectra of bulk-g-C_3N_4, CN-500, CN-520, and CN-540.

nm remained unchanged. These results indicate that TC-HCl removal by CN-540 under light is a photocatalytic process. The inset of Figure 5(e) shows the adsorption and removal of RhB (40.2%) by CN-540 under dark conditions within 140 min. It was observed that the change in absorbance of RhB was prolonged, and the position of the absorption peak near 550 nm hardly moved. This suggests that the removal of RhB by CN-540 under dark conditions is mainly through adsorption. However, as the time of visible light illumination increases, the efficiency of CN-540 photocatalytic degradation of RhB gradually increases, and the absorption peak near 550 nm has shifted towards a smaller wavelength. This shift may be due to changes in the molecular structure of RhB. Figure 5(f) illustrates the mineralization rates of CN-540 during the adsorption and photocatalytic removal processes of TC-HCl, which were calculated based on the measured TOC and are 17.7% and 51.5%, respectively. Similarly, the adsorption and photocatalytic mineralization rates for RhB by CN-540 are 22.3% and 46.6%, respectively. The experimental results indicate that CN-540 exhibits varying catalytic capabilities towards different pollutants. It can be observed from the figures that as the illumination time increases, the absorption peak intensities of the functional groups decrease, indicating that the characteristic functional groups have been cleaved.

3.3 Photocatalytic Mechanism

To reveal the active species in the photocatalytic reduction of Cr(VI) by CN-540 photocatalyst, ammonium oxalate (AO), isopropanol (IPA), and benzoquinone (BQ) were introduced to capture holes (h^+), hydroxyl radicals ($\cdot OH$), and superoxide radicals ($\cdot O_2^-$), respectively. Figure 6(a) shows that after the addition of AO, IPA, and BQ, the reduction rates of CN-540 for Cr(VI) decreased to 12.6%, 7.82%, and 26.5%, respectively, indicating that h^+, $\cdot OH$, and $\cdot O_2^-$ all play essential roles in the reduction process of Cr(VI). Therefore, it can be inferred that h^+, $\cdot OH$, and $\cdot O_2^-$ act as active radicals in the photocatalytic reaction.

It has been shown that a relatively weak PL peak typically indicates a lower recombination rate of photogenerated holes and electron pairs in semiconductor photocatalysts [30,31]. The PL emission spectral intensities shown in Figure 6b decrease in bulk-g-C_3N_4 > CN-500 > CN-520 > CN-540, indicating that thermal etching in the air atmosphere can improve the separation efficiency of photogenerated electrons and holes. Transient photocurrent (TPC) and electrochemical impedance spectroscopy (EIS) were used to evaluate the generation and separation of interfacial charges and to investigate further the separation and migration of photogenerated electrons and holes in the photocatalytic process. According to the Nyquist plots, the smaller the semicircle diameter, the smaller the carrier transfer resistance of the sample [30]. The Nyquist plots shown in Figure 7(a) indicate that the charge transfer resistances of the CN-500, CN-520, and CN-540 samples are smaller than that of bulk-g-C_3N_4, with CN-540 having the most minor charge transfer resistance. The transient photocurrent results in Figure 7(b) show that the current density of the CN-540 material is the highest, confirming its fastest separation efficiency of photogenerated carriers.

Figure 8 presents the Mott-Schottky (M-S) plots for bulk-g-C_3N_4 and CN-540. The positive slopes in the plots indicate that both bulk-g-C_3N_4 and CN-540 are n-type semiconductors [32] and that the thermal exfoliation in the air atmosphere has not changed the semiconductor type of g-C_3N_4.

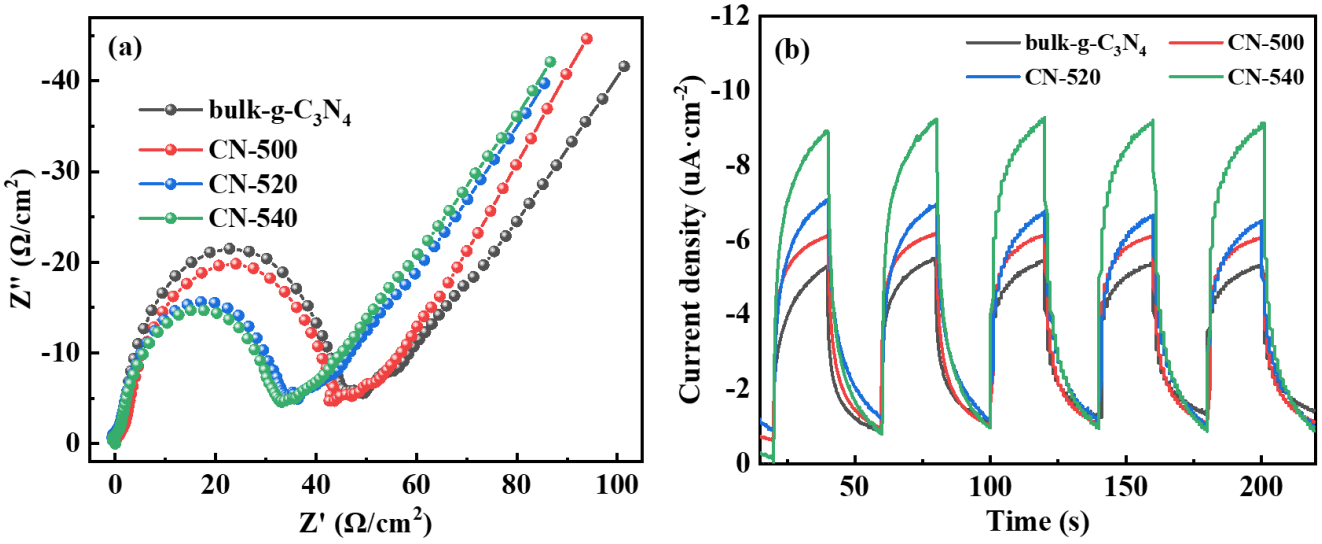

Figure 7. (a) EIS, (b) *i-t* plots for bulk-g-C_3N_4, CN-500, CN-520, and CN-540.

Using the extrapolation method where $(1/C)^2 = 0$, the flat band potentials (E_{FB}) of bulk-g-C_3N_4 and CN-540 (*vs*. Ag/AgCl) are determined to be –0.75 and –0.76 eV, respectively. According to E_{FB}（*vs*. NHE) = E_{FB} (*vs*. SCE) + 0.222 + 0.0592 × *p*H [33], where the potential of the reference electrode AgCl/Ag is 0.222 V, and the conduction band edge (E_{CB}) is typically 0.10 to 0.3 eV lower than the flat band potential (E_{FB}) of n-type semiconductors (this article takes 0.3), the E_{CB} (*vs*. NHE) of bulk-g-C_3N_4 and CN-540 are calculated to be –0.414 eV and –0.424 eV, respectively. Furthermore, based on the equation $E_{VB} = E_g + E_{CB}$, the valence band potentials (E_{VB}) of bulk-g-C_3N_4 and CN-540 (*vs*. NHE) are calculated to be +2.286 and +2.236 eV, respectively.

Given that the valence band potentials of bulk-g-C_3N_4 (2.286 eV) and CN-540 (2.236 eV) are higher than the oxidation potentials of hydroxyl radicals (•OH/OH^-, 1.99 eV) and oxygen evolution (O_2/H_2O, 1.23 eV) [34,35], both are capable of utilizing holes (h^+) to oxidize water (H_2O) to produce oxygen (O_2). The conduction band potentials of bulk-g-C_3N_4 (–0.414 eV) and CN-540 (–0.424 eV) are both more negative than the reduction potential of superoxide ($O_2/•O_2^-$, –0.33 eV) [34,35], indicating that oxygen-rich CN-540 is more likely to generate superoxide radicals (•O_2^-). Therefore, based on the band structure and the results of active species trapping experiments, we have proposed the photocatalytic mechanism for reducing Cr(VI) by CN-540 under visible light, as shown in Figure 9.

$$g\text{-}C_3N_4 + h\nu \rightarrow h^+ + e^- \quad (4)$$

$$h^+ + H_2O \rightarrow O_2 + H_2 \quad (5)$$

$$e^- + O_2 \rightarrow •O_2^- \quad (6)$$

$$h^+ + H_2O \rightarrow •OH \quad (7)$$

$$h^+ + •OH \rightarrow H_2O + CO_2 \quad (8)$$

$$e^- + Cr(VI) \rightarrow Cr(III) \quad (9)$$

$$•O_2^- + Cr(VI) \rightarrow Cr(III) + O_2 \quad (10)$$

4. Conclusions

This study has regulated the microstructure of g-C_3N_4 through thermal exfoliation in an air atmosphere, significantly enhancing its photocatalytic performance. The experimental results indicate that the CN obtained through thermal exfoliation treatment has reduced crystal grain size, decreased bandgap width, formed certain nitrogen-vacancy defects, and increased surface oxygen content, enhancing visible light absorption capability. In particular, the CN-540 sample exhibited a 96.9% reduction rate of Cr(VI), and its reaction rate constant was constant at 6.25 times that of the original g-C_3N_4. The photocatalytic degradation and mineralization rates for TC-HCl by CN-540 are 66.7% and 51.5%, Similarly, RhB was 60.6% and 46.6%, respectively. This indicates that CN-540 possesses good photocatalytic oxidation and reduction performance. Through transient photocurrent response and electrochemical impedance spectroscopy tests, it was confirmed that CN-540 has the best separation and transport efficiency of

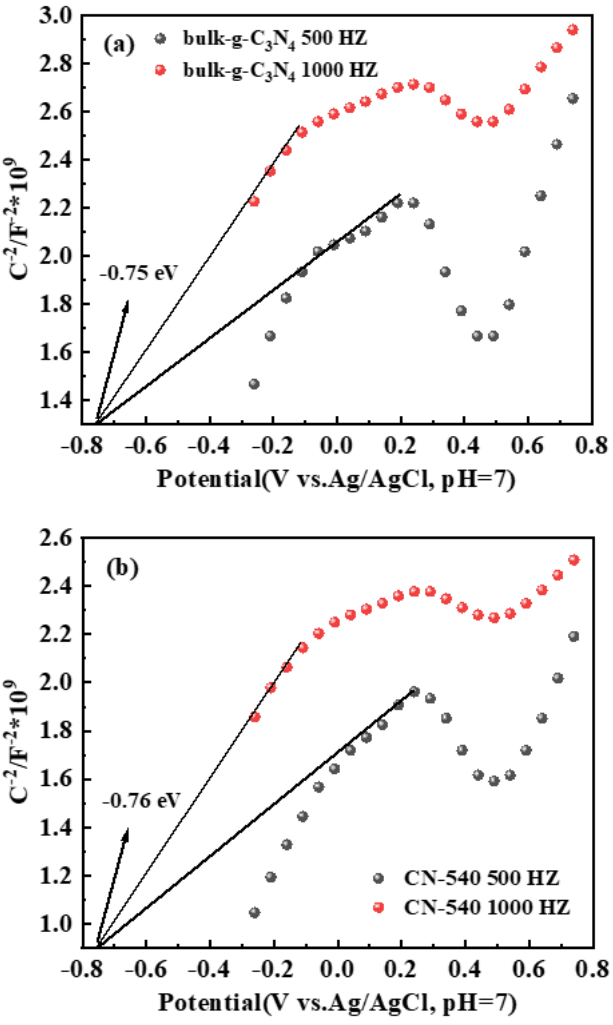

Figure 8. Mott-Schottky (M-S) plots for bulk-g-C_3N_4 and CN-540.

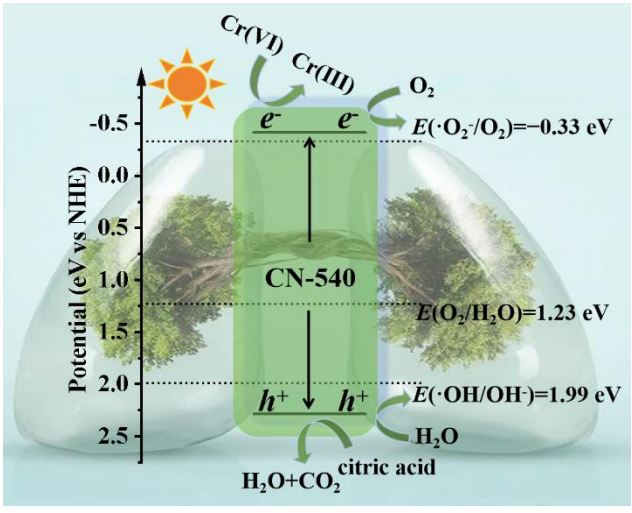

Figure 9. Schematic diagram of the photocatalytic Cr(VI) reduction by CN-540 under visible light.

photogenerated carriers. This study provides experimental evidence for optimizing the photocatalytic performance of g-C_3N_4 through thermal exfoliation strategies and offers new ideas for developing efficient photocatalysts.

CRediT Authorship Contribution Statement

Xinshan Zhao and Yuanyuan Luo: Investigation, original draft, and Writing. Junwei Yu and Tingyu Meng: Formal analysis and Investigation. Zhao Li and Lin Tian: Revision and Funding. Yanzhen Fu and Limei Sun: Review and editing. Jing Li: Supervision, Design, Revision & Funding.

Acknowledgments

This research was financially supported by the Natural Natural Science Foundation of China (NO. 22202169), the Science and Technology Project of Xuzhou (NO. KC21286), and Innovation and entrepreneurship projects for college students (xcx2024002).

References

[1] Zhu, J., Zhang, Y., Shen, L., Li, J., Li, L., Zhang, F., Zhang, Y. (2022). Hydrothermal synthesis of Nb^{5+}-doped $SrTiO_3$ mesoporous nanospheres with greater photocatalytic efficiency for Cr(VI) reduction. *Powder Technology*, 410, 117886. DOI: 10.1016/j.powtec.2022.117886.

[2] Huang, Q., Hu, J., Hu, Y., Liu, J., He, J., Zhou, G., Hu, N., Yang, Z., Zhang, Y., Zhou, Y., Zou, Z. (2022). Simultaneously enhanced photocatalytic cleanup of Cr(VI) and tetracycline via a $ZnIn_2S_4$ nanoflake-decorated 24-faceted concave MIL-88B (Fe) polyhedron S-scheme system. *Environmental Science: Nano*, 9(12), 4433-4444. DOI: 10.1039/d2en00781a.

[3] Yan, X., Zhang, N., Liu, Z., Du, C. (2024). Two-step calcination synthesis of 1T/2H mixed-phase MoS_2/g-C_3N_4 with sulfur defects for efficient removal of Cr(VI) from water. *Journal of Molecular Structure*, 1300, 137262. DOI: 10.1016/j.molstruc.2023.137262.

[4] Wei, H., Wen, Y., Zhang, Y. (2017). Nitric acid-assisted one-step solvothermal synthesis of visible-light-active N-doped ThO_2 for use as a potential photocatalyst in the reduction of Cr(VI). *Catalysis Communications*, 99, 66-70. DOI: 10.1016/j.catcom.2017.05.030.

[5] Wang, C., Yang, G., Shi, W., Matras-Postolek, K., Yang, P. (2021). Construction of 2D/2D MoS_2/g-C_3N_4 heterostructures for photoreduction of Cr(VI). *Langmuir*, 37(20), 6337-6346. DOI: 10.1021/acs.langmuir.1c00929.

[6] Zhang, Y., Liu, C., Nian, P., Ma, H., Hou, J., Zhang, Y. (2024). Facile preparation of high-performance hydrochar/TiO_2 heterojunction visible light photocatalyst for treating Cr(VI)-polluted water. *Colloids and Surfaces A: Physicochemical and Engineering Aspects*, 681, 132775. DOI: 10.1016/j.colsurfa.2023.132775.

[7] Chen, Y., Li, A., Fu, X., Peng, Z. (2022). One-step calcination to gain exfoliated g-C_3N_4/MoO_2 composites for high-performance photocatalytic hydrogen evolution. *Molecules*, 27(21), 7178. DOI: 10.3390/molecules27217178.

[8] Yang, Y., Yan, J., Zhang, Y., Xing, S., Ran, J., Ma, Y., Li, X. (2024). S/P co-doped g-C_3N_4 with secondary calcination for excellent photocatalytic performance. *International Journal of Hydrogen Energy*, 51, 962-974. DOI: 10.1016/j.ijhydene.2023.09.083.

[9] Yu, Q., Xu, Q., Li, H., Yang, K., Li, X. (2019). Effects of heat treatment on the structure and photocatalytic activity of polymer carbon nitride. *Journal of Materials Science*, 54(23), 14599-14608. DOI: 10.1007/s10853-019-03895-w.

[10] Rehman, Z.U., Bilal, M., Butt, F.K., Rehman, S.U., Asghar, Z., Zheng, K., Zhang, Y., Xu, X., Hou, J., Wang, X. (2024). Selenium doping to improve internal electric field for excellent photocatalytic efficiency of g-C_3N_4 nanosheets. *Separation and Purification Technology*, 350, 128001. DOI: 10.1016/j.seppur.2024.128001.

[11] Nguyen, T.T.A., Dao, T.C.V., Vu, A.T. (2024). Controlling the physical properties of Ag/ZnO/g-C_3N_4 nanocomposite by the calcination procedure for enhancing the photocatalytic efficiency. *Ceramics International*, 50(9), 14292-14306. DOI: 10.1016/j.ceramint.2024.01.336.

[12] Wang, T., Yang, W., Chang, L., Wang, H., Wu, H., Cao, J., Fan, H., Wang, J., Liu, H., Hou, Y., Zhang, R., Yang, Z., Zhu, H., Kong, C. (2022). One-step calcination synthesis of accordion-like MXene-derived TiO_2@C coupled with g-C_3N_4: Z-scheme heterojunction for enhanced photocatalytic NO removal. *Separation and Purification Technology*, 285, 120329. DOI: 10.1016/j.seppur.2021.120329.

[13] Zhang, X., Yuan, L., Zhang, Y., Shu, X., Li, R., Deng, Q., Zhang, Z., Yang, R. (2024). Synthesis and photocatalytic performance investigation of an NH_4Cl-assisted two-step calcination method for modified gC_3N_4. *Reaction Chemistry & Engineering*. DOI: 10.1039/d4re00151f.

[14] Cao, R., Yuan, H., Yang, N., Lu, Q., Xue, Y., Zeng, X. (2024). Enhanced photocatalytic hydrogen production utilizing few-layered 1T-WS_2/g-C_3N_4 heterostructures prepared with one-step calcination route. *Fuel*, 357, 129808. DOI: 10.1016/j.fuel.2023.129808.

[15] Zhang, Q., Liu, S., Zhang, Y., Zhu, A., Li, J., Du, X. (2016). Enhancement of the photocatalytic activity of g-C_3N_4 via treatment in dilute NaOH aqueous solution. *Materials Letters*, 171, 79-82. DOI: 10.1016/j.matlet.2016.02.043.

[16] De Medeiros, T.V., Porto, A.O., Bicalho, H.A., González, J.C., Naccache, R., Teixeira, A.P.C. (2021). The effects of chemical and thermal exfoliation on the physico-chemical and optical properties of carbon nitrides. *Journal of Materials Chemistry C*, 9(24), 7622-7631. DOI: 10.1039/d1tc01734a.

[17] Nguyen, T.K.A., Pham, T.T., Gendensuren, B., Oh, E.S., Shin, E.W. (2022). Defect engineering of water-dispersible g-C_3N_4 photocatalysts by chemical oxidative etching of bulk g-C_3N_4 prepared in different calcination atmospheres. *Journal of Materials Science & Technology*, 103, 232-243. DOI: 10.1016/j.jmst.2021.07.013.

[18] Liu, S., Sun, H., Ang, H.M., Tade, M.O., Wang, S. (2016). Integrated oxygen-doping and dye sensitization of graphitic carbon nitride for enhanced visible light photodegradation. *Journal of colloid and interface science*, 476, 193-199. DOI: 10.1016/j.jcis.2016.05.026.

[19] Yu, Q., Xu, Q., Li, H., Yang, K., Li, X. (2019). Effects of heat treatment on the structure and photocatalytic activity of polymer carbon nitride. *Journal of Materials Science*, 54(23), 14599-14608. DOI: 10.1007/s10853-019-03895-w.

[20] Kang, X., Kang, Y., Hong, X., Sun, Z., Zhen, C., Hu, C., Liu, G., Cheng, H. (2018). Improving the photocatalytic activity of graphitic carbon nitride by thermal treatment in a high-pressure hydrogen atmosphere. *Progress in Natural Science: Materials International*, 28(2), 183-188. DOI: 10.1016/j.pnsc.2018.02.006.

[21] Yu, H., Yu, Z., Chen, F., Li, W., Qi, L., Zhu, F., Zhu, B., Zhang, S., Zhao, Z., Zheng, J. (2024). Optimization of Ag single atom dispersed graphitic carbon nitride for enhanced catalytic performance in the degradation of rhodamine B and tetracycline. *Materials Research Bulletin*, 170, 112553. DOI: 10.1016/j.materresbull.2023.112553.

[22] Mishra, K.P., Gogate, P.R. (2010). Intensification of degradation of Rhodamine B using hydrodynamic cavitation in the presence of additives. *Separation and Purification Technology*, 75(3), 385-391. DOI: 10.1016/j.seppur.2010.09.008.

[23] Nie, Y., Zhao, C., Zhou, Z., Kong, Y, Ma, J. (2023). Hydrochloric acid-modified fungi-microalgae biochar for adsorption of tetracycline hydrochloride: Performance and mechanism. *Bioresource Technology*, 383, 129224, DOI: 10.1016/j.biortech.2023.129224.

[24] Ma, C., Aryee, A.A., Zhu, K., Wang, R., Han, R. (2024). Adsorption and catalytic degradation of tetracycline hydrochloride by HCNTs /$MnFe_2O_4$. *Journal of Environmental Chemical Engineering*, 12, 113156. DOI: 10.1016/j.jece.2024.113156.

[25] Guo, F., Shi, W., Wang, H., Huang, H., Liu, Y., Kang, Z. (2017). Fabrication of a $CuBi_2O_4$/g-C_3N_4 p–n heterojunction with enhanced visible light photocatalytic efficiency toward tetracycline degradation. *Inorganic Chemistry Frontiers*, 4(10), 1714-1720. DOI: 10.1039/c7qi00402h.

[26] Hosseini, S.F., Dorraji, M.S.S., Rasoulifard, M.H. (2023). Boosting photo-charge transfer in 3D/2D TiO_2@Ti_3C_2 MXene/Bi_2S_3 Schottky/Z-scheme heterojunction for photocatalytic antibiotic degradation and H_2 evolution. *Composites Part B: Engineering*, 262, 110820. DOI: 10.1016/j.compositesb.2023.110820.

[27] Li, S., Zhao, W., Xiong, D., Ye, Y., Ma, J., Gu, Y. (2023). g-C_3N_4/TiO_2 uniformly distributed microspheres: preparation for enhanced photocatalytic performance by co-calcination. *Journal of Materials Science: Materials in Electronics*, 34(1), 47. DOI: 10.1007/s10854-022-09391-3.

[28] Niu, P., Qiao, M., Li, Y., Huang, L., Zhai, T. (2018). Distinctive defects engineering in graphitic carbon nitride for greatly extended visible light photocatalytic hydrogen evolution. *Nano Energy*, 44, 73-81. DOI: 10.1016/j.nanoen.2017.11.059.

[29] Wu, J., Li, N., Fang, H. B., Li, X., Zheng, Y.Z., Tao, X. (2019). Nitrogen vacancies modified graphitic carbon nitride: Scalable and one-step fabrication with efficient visible-light-driven hydrogen evolution. *Chemical Engineering Journal*, 358, 20-29. DOI: 10.1016/j.cej.2018.09.208.

[30] Yu, Y., Chen, D., Xu, W., Fang, J., Sun, J., Liu, Z., Chen, Y., Liang, Y., Fang, Z. (2021). Synergistic adsorption-photocatalytic degradation of different antibiotics in seawater by a porous g-C_3N_4/calcined-LDH and its application in synthetic mariculture wastewater. *Journal of Hazardous Materials*, 416, 126183. DOI: 10.1016/j.jhazmat.2021.126183.

[31] Yu, Q., Xu, Q., Li, H., Yang, K., Li, X. (2019). Effects of heat treatment on the structure and photocatalytic activity of polymer carbon nitride. *Journal of Materials Science*, 54(23), 14599-14608. DOI: 10.1007/s10853-019-03895-w.

[32] Bai, Y., Mao, W., Wu, Y., Gao, Y., Wang, T., Liu, S. (2021). Synthesis of novel ternary heterojunctions via Bi_2WO_6 coupling with CuS and g-C_3N_4 for the highly efficient visible-light photodegradation of ciprofloxacin in wastewater. *Colloids and Surfaces A: Physicochemical and Engineering Aspects*, 610, 125481. DOI: 10.1016/j.colsurfa.2020.125481.

[33] Paramanik, L., Subudhi, S., Parida, K.M. (2022). Visible light active titanate perovskites: An overview on its synthesis, characterization and photocatalytic applications. *Materials Research Bulletin*, 155, 111965. DOI: 10.1016/j.materresbull.2022.111965.

[34] Pang, X., Xue, S., Zhou, T., Xu, Q., Lei, W. (2022). 2D/2D nanohybrid of Ti_3C_2 MXene/WO_3 photocatalytic membranes for efficient water purification. *Ceramics International*, 48, 3659–3668. DOI: 10.1016/j.ceramint.2021.10.147.

[35] Liu, K., Zhang, H., Fu, T., Wang, L., Tang, R., Tong, Z., Huang, X. (2022). Construction of BiOBr/Ti_3C_2/exfoliated montmorillonite Schottky junction: New insights into exfoliated montmorillonite for inducing MXene oxygen functionalization and enhancing photocatalytic activity. *Chemical Engineering Journal*, 438, 135609. DOI: 10.1016/j.cej.2022.135609.